2021

Large-scale synthesis of compressible and re-expandable three-dimensional nanofiber matrices

Alec McCarthy

Lorenzo Saldana

Daniel McGoldrick

Johnson V. John

Mitchell Kuss

See next page for additional authors

Authors

Alec McCarthy, Lorenzo Saldana, Daniel McGoldrick, Johnson V. John, Mitchell Kuss, Shixuan Chen, Bin Duan, Mark A. Carlson, and Jingwei Xie

Received: 9 December 2020 | Revised: 15 January 2021 | Accepted: 1 February 2021

Open Access CC-BY

DOI: 10.1002/nano.202000284

RESEARCH ARTICLE

Nano Select WILEY

Large-scale synthesis of compressible and re-expandable three-dimensional nanofiber matrices

Alec McCarthy[1] | **Lorenzo Saldana**[1] | **Daniel McGoldrick**[2] | **Johnson V. John**[1] | **Mitchell Kuss**[1,3] | **Shixuan Chen**[1] | **Bin Duan**[1,3] | **Mark A. Carlson**[5,6] | **Jingwei Xie**[1,4]

[1] Department of Surgery – Transplant and Mary & Dick Holland Regenerative Medicine Program, College of Medicine, University of Nebraska Medical Center, Omaha, Nebraska, USA

[2] Department of Computer Science, School of Computing & Design, California State University - Monterey Bay, Seaside, California, USA

[3] Division of Cardiology, Department of Internal Medicine, University of Nebraska Medical Center, Omaha, Nebraska, USA

[4] Department of Mechanical and Materials Engineering, College of Engineering, University of Nebraska-Lincoln, Lincoln, Nebraska, USA

[5] Department of Surgery-General Surgery, College of Medicine, University of Nebraska Medical Center, Omaha, Nebraska, USA

[6] Surgery Department, Nebraska-Western Iowa Health Care System, Omaha, Nebraska, USA

Correspondence
Jingwei Xie, Department of Surgery – Transplant and Mary & Dick Holland Regenerative Medicine Program, College of Medicine, University of Nebraska Medical Center, Omaha, NE 68198, USA.
Email: jingwei.xie@unmc.edu

Funding information
National Institute of General Medical Sciences; Congressionally Directed Medical Research Programs

Abstract

Due to their biomimetic properties, electrospun nanofibers have shown great potential in many biomedical fields. However, traditionally-produced nanofibers are typically two-dimensional (2D) membranes limiting their applications. Herein, we report a large-scale synthesis of compressible and re-expandable three-dimensional (3D) nanofiber matrices for potential biomedical applications. The reproducible mass production of such matrices is achieved using a multiple-emitter electrospinning machine with a controlled environment (e.g., temperature, humidity, and air flow rate) followed by an innovative gas-foaming expansion. The modified 20-emitter circular array with 3D-printed needle caps is capable of maintaining stable Taylor cones under extremely high flow rates. The introduction of such an emitter array allows for the production rate of 3D nanofiber matrices to increase by over 800 times while retaining the desired morphological, mechanical, and absorptive properties when compared to ones generated by a single-nozzle electrospinning setup. Taken together, a feasible, optimized method has been demonstrated for scaling up production of shape-recoverable, expansile nanofiber matrices, representing a step towards translating such materials into preclinical, large animal testing, clinical trials, and eventually clinical applications.

KEYWORDS
electrospinning, hemostasis, large-scale, nanofiber matrices, shape-recoverable

1 | INTRODUCTION

Nanofibers have garnered much attention in recent decades in many fields such as biomedical and food sciences, environmental engineering, and energy.[1–5] There exist many methods to produce nanofibers, such as phase separation, self-assembly, electrospinning, solution blow spinning, rotary/centrifugal jet spinning, pulling, and electrohydrodynamic direct writing.[6,7] Among them, electrospinning, which uses an electric field to draw polymer solutions into continuous nanofibers that are subsequently collected on grounded collectors, is considered one of the most practical methods due to its flexibility, low cost, and ease of use.[8] Due to the intrinsic property of electrospinning, electrospun nanofibers are often deposited to the surface of collectors, resulting in the formation of two-dimensional (2D) nanofiber mats rather than three-dimensional (3D) objects.[5] Such 2D mats having limited thickness are densely packed, leading to small pore sizes (often smaller than the dimension of mammalian cells) and inhibition of cellular penetration.[9]

To overcome the above-mentioned problems, different strategies have been developed to address the planar limitations of electrospun nanofiber materials based on sacrificial templating, charge accumulation/electrostatic repulsion, design of special collectors, ultrasound post-processing, and short nanofiber assembly.[9–15] However, these 3D objects were associated with inadequate control of shapes and porosities. In addition, 3D objects produced by these methods were mainly composed of random nanofibers or some specific materials. Our group and others developed an innovative gas-foaming technology for expanding 2D nanofiber membranes into 3D scaffolds.[16–19] Such scaffolds enabled the formation of a layered structure, controllable porosity, and maintenance of nanofiber alignment. Recently, inspired by the solids-of-revolution concept, gas-foaming expansion technology was used to transform electrospun nanofiber mats into 3D objects with hierarchically assembled nanofibers with controlled alignment and porosity.[20] More recently, in combination with 3D molds and the gas-foaming expansion technique, 3D nanofiber objects with predesigned shapes and controlled fiber alignment and porosity can be achieved.[21] The expanded nanofiber scaffolds promoted cell infiltration, collagen deposition and new vascularization after subcutaneous implantation. In addition, the expanded nanofiber matrices after coating with 0.5% gelatin showed superelastic property, high capability of blood absorption, and short blood clotting time.[22] Most recently, 3D nanofiber assemblies with structural and compositional gradients were also generated through the transformation of 2D electrospun membranes based on the gas-foaming expansion technique.[23]

However, the above-mentioned studies involved the use of the traditional laboratory single-nozzle electrospinning setup and gas-foaming expansion to generate 3D nanofiber matrices, resulting in slow production and a low yield. Traditional electrospinning setups includes a syringe, a needle, a syringe pump, a high voltage generator, and a grounded collector.[24] Though easy to assemble, this conventional setup often produced 0.01–0.1 g h^{-1} of nanofibers, falling well short of a practical method to produce large quantities of nanofibers.[25] To translate these materials to preclinical large animal tests and clinical trials, there is a need to increase the production rate of 3D nanofiber matrices. Industrial electrospinning setups may meet the scale-up production needs, but are often too large and expensive to be practical for experimental research. In addition, it is unknow whether the 2D nanofiber membranes produced by industrial electrospinning equipment can be transform into 3D objects with hierarchical assemblies.

Many methods have been proposed to scale up the production rate, ranging from a variety of nozzle modifications to free surface and dynamic electrospinning.[26,27] While each method demonstrates improved production rates compared to a traditional set up, most suffer from a lack of environmental regulation, control of fiber orientation, consistency, and reproducibility. For instance, AC voltage electrospinning generates multiple Taylor cones that orient in different directions, rapidly creating large plumes of nanofibers, but doing so in a way that makes controlling fiber alignment difficult.[28,29] In many cases, ensuring nanofiber morphological uniformity and alignment is crucial for material functionality, particularly in biomedical applications.[30,31] In this study, we sought to scale up the production of expanded 3D nanofiber matrices through the use of an electrospinning setup having multiple emitters modified with 3D-printed needle caps. To achieve this goal, the produced 2D mats should retain the same features (e.g., fiber diameter, fiber alignment, no fusion between fibers) as the ones produced by the single-nozzle electrospinning setup. The mats should also be able to expand to the similar degree as the ones produced by the traditional setup *via* the gas-foaming technology.[22] Additionally, the structure of expanded 3D matrices should be akin to the ones produced by traditional laboratory electrospinning and gas-foaming, exhibiting comparable performance in terms of water absorption and shape-recovery capability.[22] Optimizing fabrication parameters in this complex system could enable rapid production of expanded 3D nanofiber matrices, bringing this emerging material towards pre-clinical large animal studies and eventually clinical trials and applications.

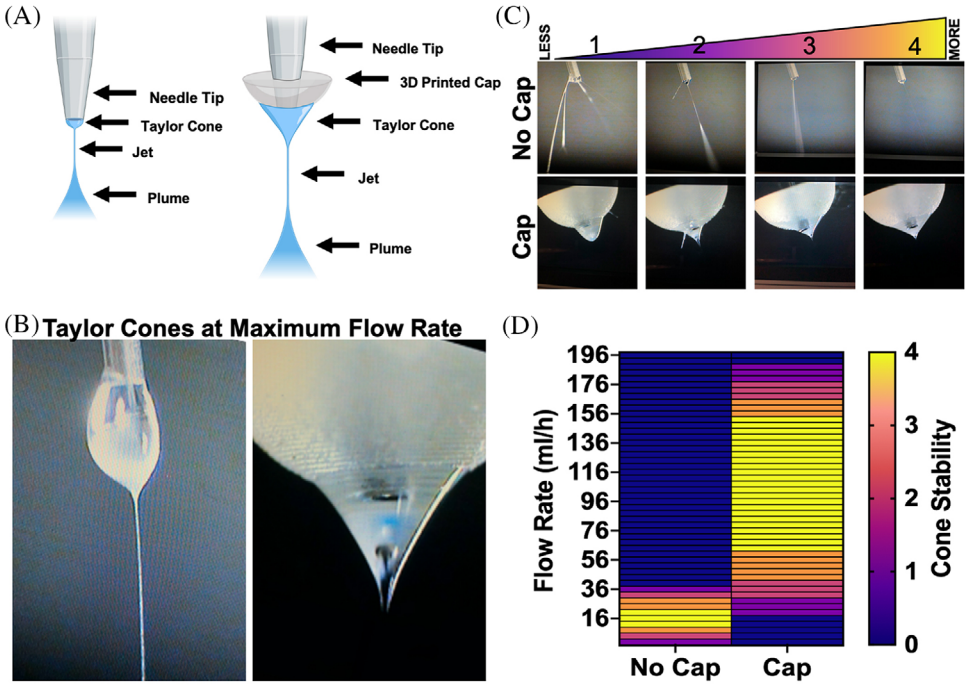

FIGURE 1 Taylor cone stability while spinning 10% PCL + 0.1% F-127 with and without 3D printed needle caps. A, A schematic representation and description of the elements of a Taylor cone during electrospinning with and without a 3D printed cap. B, Taylor cone morphology at maximum spinnable flow rates on a traditional and capped set up. C, Qualitative scale used to categorize the stability of Taylor cones at increasing flow rates (stability increases numerically from least to most stable). D, Heat map contrasting ranges of Taylor Cone stability of capless and capped needles at 10 kV electrospinning

2 | RESULTS

2.1 | Role of 3D printed caps in Taylor cone stability

While simply electrospinning from more emitters is one method to enhance production rate, other adaptations manipulating the mechanics of Taylor cones may serve to further enhance the continuous and reproducible production of nanofibers. In a previous study, 3D printed needle caps were used to enhance the stability of electrosprayed liquid solutions with high flow rates.[32] Applying the same principle to electrospinning, we speculated that adding 3D printed caps to emitters could enhance Taylor cone stability under exceptionally high flow rates. Unlike the study introducing this concept for electrospraying,[32] here it was vital to maintain an undisrupted flow of polymer jet solution for continuous nanofiber production. The addition of the 3D printed caps enhanced electrospinning in several ways. Similar to the theory proposed by Morad et al.,[32] the addition of the caps prevent the polymer solution from wicking up the outside of the needle due to capillary action imparted by the metal-polymer solution interface. Preventing the polymer solution from climbing the outside of the emitter tip both reduces capillary forces acting opposite that of gravity and subsequently localizes the polymer solution towards the jetting region while reducing pendant-shaped cones from forming.[32] Further, the addition of the needle caps increases both the surface area of the emitter-cone interface and the meniscus diameter (and subsequent volume) of the Taylor cone. Previous investigations have shown that large volume Taylor cones with larger meniscal diameters (cone bases) result in longer jetting regions and experience enhanced geometric stability by reducing circulating flow regions in the Taylor cone during electrospinning.[33–35] The different configurations of the electrospinning emitters and their relative relation to jetting regions and Taylor cone geometry is visualized in Figure 1A. At maximum flow rates for both uncapped and capped emitters, the shape of the Taylor cones were markedly different. Without a cap, a pendant shaped Taylor cone was present, which is geometrically unfavorable for electrospinning, though with a cap, even at maximum flow rates, the Taylor cone retained its conical shape, making dripping and secondary cone formation less frequent (Figure 1B). The qualitative assignment of cone stabilities at different flow rates demonstrated the advantage of electrospinning with caps, as not only higher flow rates were sustained, but pristine spinning was maintained over a much larger range of flow rates (Figure 1C and D).

FIGURE 2 The Fluidnatek LE-100 used for nanofiber mat production and the 20-emitter circular array with 3D printed needle caps attached

2.2 | Scaling-up production of PCL nanofiber mats

Expanded 3D nanofiber matrices produced previously showed immense promise in biomedical applications (e.g., as hemostatic devices to treat hemorrhage).[21,22,33] However, their production yield was low, which made transitioning to large animal studies and clinical trials impractical. In order to accelerate the production rate, an electrospinning machine, the Fluidnatek LE-100 (LE-100), was employed (Figure 2). The LE-100 offers a variety or enhanced controls (e.g., temperature, humidity, and air flow rate), including multiple emitters. To enhance stability of the electrospinning jet, 3D printed caps were fixed to the end of each needle in a 20-emitter circular array (Figure 2). Since using a setup with multiple emitters introduced multiple new variables, it was crucial to ascertain that fiber alignment and morphology did not dramatically differ between setups. The fabrication parameters for each setup were shown in Table 1. Figure 3A-C shows the appearance of each device's Taylor cone at optimized spinning conditions. SEM images and accompanying orientation analysis demonstrated no distinct morphological differences between setups (Figure 3D-F). Fibers produced by the single nozzle, single nozzle + cap, and array + caps electrospinning set ups had mean diameters of 1.01 ± 0.41, 1.15 ± 0.47, and 1.105 ± 0.48 μm, respectively, and did not significantly vary ($P = .1121$, $n = 1000$) (Figure 3G and H). Additionally, alignment analysis indicated that the single nozzle + cap set up had the most well-aligned fibers with a peak orientation frequency count of 24,901, followed by the array + cap setup, which had a peak orientation frequency count of 23,072, and finally the single nozzle electrospinning setup, which had a peak orientation frequency count of 18,278 (Figure 3I). Mats produced using single nozzle + cap had the highest degree of alignment due to the improved Taylor con stability and lack of interfering fibers from multiple emitters. However, fiber mats produced from the LE-100 array + cap showed a similar degree of orientation and distribution frequency, suggesting that, despite some interference from multiple emitters, fibers retained excellent alignment. Optimized parameters for the LE-100 were determined by Taylor cone stability and fiber quality (e.g., diameter and alignment) of the nanofiber mats.

2.3 | Effect of applied voltages on the fiber fabrication

Fiber morphology varied dramatically when applied voltage was changed. Under higher voltages, the jet plumes were smaller and occupied less space, leaving less room for interacting with adjacent plumes (Figure 4A and B). Subsequently, at higher voltages (e.g., 60 kV), the fibers had significantly smaller diameters and tighter degree of alignment as evident by SEM (Figure 4E-H). Conversely, the jet under lower voltages had wider plumes that frequently contacted adjacent plumes, likely resulting in the fusion of some fibers (Figure 4C and D). At lower voltages (e.g., 30 kV), fibers had larger diameters with a broader alignment distribution, likely imparted by fused fibers (Figure 4F and H). Additionally, under lower voltages, the jet plumes frequently contacted while still in air, causing the fibers to fall towards the collector before complete solvent evaporation, thus leading to slightly larger fibers with multiple fusion sites. At both 60 and 30 kV, the Taylor cones were stable, but the jet plumes varied, as indicated by the outline of the plumes in Figure 4A and C. During spinning at lower voltages, the larger plumes caused nanofibers to cross as indicated by the fibers in red in Figure 4D and fall out from their spinning pathways, but at higher voltages, the jet plumes did not contact and thus did not cause fusion (Figure 4B), allowing for total solvent evaporation. The Taylor cones varied in length based on voltage such

TABLE 1 The parameters for different electrospinning setups

Setting	Single-nozzle	Single-nozzle + Cap	Array + Cap
Solution [% w v^{-1}]	10% PCL + 1.0% F-127	10% PCL + 1.0% F-127	10% PCL + 1.0% F-127
Flow Rate [mL h^{-1}]	0.7	7.5	150
Voltage [kV]	18	14	60
Temperature [°C]	23	29	29
Relative Humidity [%]	55	65	65
Air Flow [m^3 h^{-1}]	25	150	150
Distance [cm]	18	22	22
Drum Linear Velocity [m s^{-1}]	2.9	2.1	2.1
Syringe Size [cc]	10	10	100
X Sweep	stationary	70–230 mm at 55 mm s^{-1}	70–230 mm at 55 mm s^{-1}
Productivity [peanuts h^{-1}]	0.48	5.9	420

Single-nozzle: single stationary needle, no environmental controls; Single-nozzle + Cap: LE-100 with single emitter and cap; and Array + Cap: LE-100 with 20 emitter array and cap.

that the jet stream was longer at 60 kV (**Video S1**) than 30 kV (**Video S2**). Taken together, higher voltages led to tighter jet plumes that did not cross, resulting in no fusion between fibers, tighter fiber alignment, and diameter distributions. Such nanofiber membranes could be suitable for expansion during the gas-foaming process.

2.4 | Comparing production efficiency

Dramatically increasing the production efficiency was the overarching goal of the study. Understanding the factors that contributed to the improved efficiency was necessary to translate the 3D nanofiber matrices to clinical settings. In the single nozzle electrospinning setup, tapering towards the edges made a majority of the mat unusable due to lack of uniformity (Figure 5Ai). Conversely, the lateral sweep enabled by the LE-100 allowed the emitter head to travel back and forth along the collecting drum, greatly reducing any edge tapering (Figure 5Aii). The overall size of the nanofiber mat produced from the LE-100 was 61 cm × 28 cm (1708 cm^2) (Figure 5Bi), while the size of the nanofiber mat produced by our previous setup was 10 cm × 10 cm (100 cm^2). After spinning, nanofiber mats from each setup were removed and the edges were trimmed until the mat thickness was uniform. Lateral sweeping allowed for 94% ± 3% of the mat to be used as compared to 32% ± 9% using our previous setup (Figure 5C) ($P < .001$). After trimming any edges off, the mats produced by LE100 were able to expand in sodium borohydride ($NaBH_4$) solution, similar to the ones produced in our previous studies (Figure 5Bii).[16,22] In addition, it is worth mentioning that the mats from Figure 4D could not expand to the same extent due to the fusion between fibers. Other than the percent of the usable nanofiber mat, the maximum stable flow rate correlated with the yield of 3D nanofiber matrices simply as a throughput parameter. A single nozzle electrospinning setup can stably spin at flow rates ranging from 0.5 to 1.0 mL h^{-1}. A single nozzle + cap setup can stably spin at flow rates ranging from 3.2 to 7.4 mL h^{-1}, and an array + cap setup can stably spin at flow rates ranging from 64.0 to 152.0 mL h^{-1}. Taking both the maximum stable flow rate and usable mat area for single nozzle, single nozzle + cap, and array + cap electrospinning setups, the production rates of 3D nanofiber matrices (1 cm × 1 cm × 7 cm) were 0.48 ± 0.22 matrices/batch, 5.90 ± 1.3 matrices/batch, and 420.00 ± 12.1 matrices/batch, respectively (Figure 5E) ($P < .0001$). The LE-100 with modified caps produced the 3D PCL nanofiber matrices nearly 875 times faster than the single nozzle electrospinning setup, marking a tremendous leap towards clinical translation and large-scale production.

2.5 | Morphology and structure of expanded 3D nanofiber matrices

For scaling up production, recapitulating the structure of the 3D nanofiber matrices produced by the single nozzle electrospinning setup is of utmost importance. Figure 6A shows a SEM image of the cross section of a LE-100-fabricated nanofiber mat before expansion, indicating about 1 mm thick and densely packed structure. Figure 6B shows a SEM image of the cross section of 3D nanofiber matrices expanded from a LE-100-fabricated nanofiber mat followed by 0.5% gelatin coating, exhibiting layered, porous structures and maintaining fiber alignment. The SEM image under higher magnification shows individual nanofibers composing pore walls (Figure 6C). Importantly, the nanofiber mats produced from the LE-100 were able

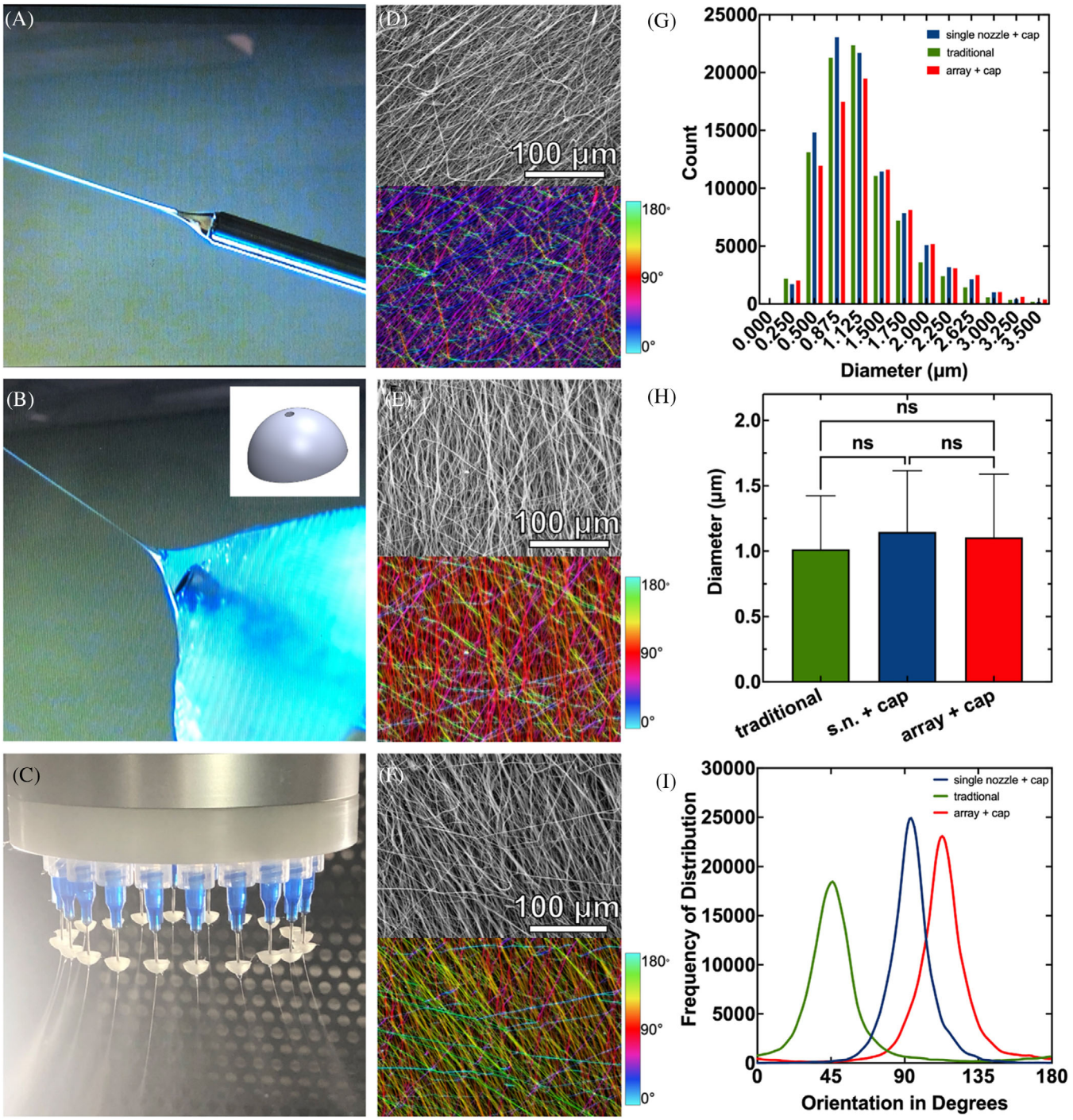

FIGURE 3 Different electrospinning setups and nanofiber morphologies and alignments. A, traditional, (B) single nozzle + cap, (C) array + cap electrospinning set ups and (D-F) the resulting SEM and orientation of electrospun nanofibers. G, The distribution frequency of fiber diameters from each electrospinning setup. H, The mean fiber diameter ($P > .05$, ns = not significant) and (I) The distribution frequency of fiber orientations from each electrospinning setup

to expand from a mean thickness of 0.105 ± 0.07 cm to an expanded thickness of 7.33 ± 0.36 cm (Figure 6D-F).

For some biomedical applications, 3D nanofiber matrices with larger dimensions may be required. To test the feasibility of scaling up the production of large 3D nanofiber matrices, nanofiber mats (10 cm × 10 cm) were prepared by cutting the membranes produced from the LE100 with modified caps. By making use of a customized mold (10 cm high), 3D nanofiber matrices with a dimension of 10 cm × 10 cm × 10 cm were successfully obtained after expansion. The matrices measured roughly 1000 cm^3 and showed uniform expansion throughout the bulk of

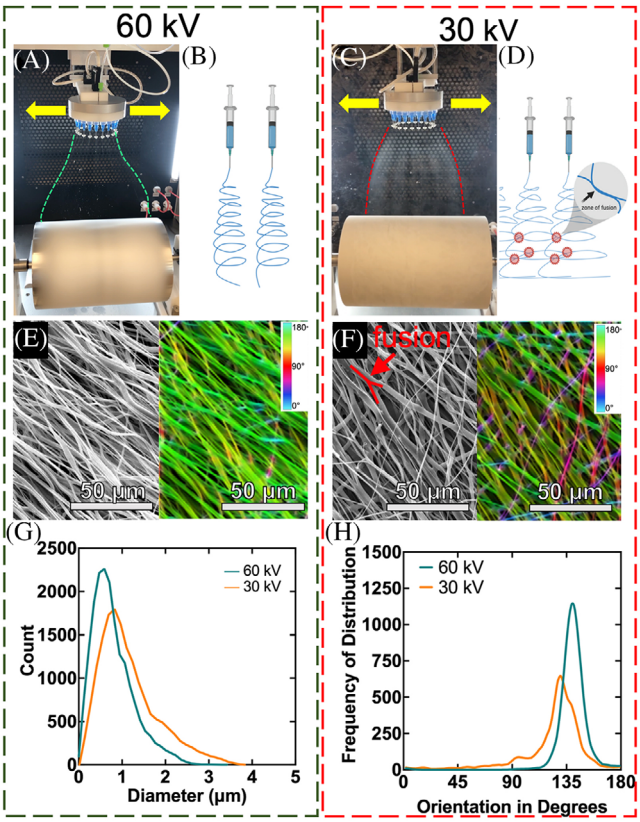

FIGURE 4 Fiber fusion as a function of applied voltage. A, Electrospinning jet plumes (indicated by green dashed line) at 60 kV and (B) schematic showing non-interaction of adjacent plumes. C, Electrospinning jet plumes (indicated by red dashed line) at 30 kV and (D) schematic representing fiber fusion between adjacent plumes. (E & F) SEM images and alignment analysis of nanofiber mats spun at (E) 60 kV and (F) 30 kV (fused nanofiber indicated by red arrow). G, Frequency distribution of fiber diameters at 60 and 30 kV. H, Frequency distribution of fiber alignments under both voltage conditions

the material (Figure 7A and B). Unlike the matrices with 1 cm × 1 cm, however, the size and orientation of the pores appeared more directionally-dependent. The pores along the X-Y axis tended to be longer, horizontally-oriented ellipsis, while the pores along the Z-Y axis tended to be more circular (Figure 7C-F). The nanofiber composition along both axes showed no distinct morphological differences (Figure 7E and F) and the sole contributing factor in the different pore shapes could be the orientation relative to fiber alignment. Pores parallel to the aligned nanofibers were longer and appeared as layers pulling apart, whereas the pores normal the aligned fibers appeared circular as the nucleating bubbles could better separate individual fibers. Similarly, we demonstrated the transformation of 2D nanofiber mats produced from the LE100 to 3D objects consisting of radially-aligned nanofibers based on the solids of revolution-inspired expansion, which further confirmed the expansion ability of 2D nanofiber mats produced by the LE-100 with modified caps (Figure S1).[20]

2.6 | Shape recovery, absorption, and re-expansion properties

Our previous studies demonstrated the superelasticity, superabsorptivity, and re-expansibility of expanded 3D nanofiber matrices produced by single nozzle electrospinning.[22] The hemostatic abilities of 3D nanofiber matrices were also determined both in vitro and in swine liver injury models.[21,22] Since we have already determined the efficacy of the 3D nanofiber matrices in hemostasis, here we sought to scale up the production of 3D nanofiber matrices which can replicate the properties of those fabricated by single nozzle electrospinning. (3D PCL nanofiber matrices produced from the LE-100 after coating with 0.5% gelatin were able to recover 95.94% of their original shape after a manual compression of roughly 90%, while uncoated matrices recovered significantly less (51.73%) of their original length ($P < .0001$) (Figure 8A-C). Gelatin-coated PCL nanofiber matrices produced from the LE-100 also demonstrated super absorptive properties, absorbing 6007% ± 385.4% of its initial weight in body-simulated fluids (BSF), while uncoated matrices absorbed a significantly lower amount (4521% ± 576.3%) of its weight ($P = .0052$) (**Video S3**) (Figure 8D and E). Additionally, gelatin-coated 3D nanofiber matrices were able to re-expand while submerged in BSF, reaching 81% ± 3.31% of its originally expanded length in 16.6 ± 1.0 seconds, while uncoated matrices were only able to recover 42% ± 6.3% of their original shape in 21.0 ± 2.5 seconds ($P = .0196$) (Figure 8F and G). Therefore, 3D nanofiber matrices produced from the LE-100 demonstrated similar superelastic and shape recovering properties as the matrices previously fabricated by single nozzle electrospinning.[22]

3 | DISCUSSION

Many innovative materials fail to progress out of laboratory settings, most commonly due to the inability to easily scale up the fabrication while retaining desired properties.[34,36] In particular, engineering micro- or nanomaterials often requires precise control over individual fabrication parameters. 3D nanofiber matrices have demonstrated great potential in many biomedical applications including hemostasis, tissue modeling, tissue repair, and regeneration, wound healing.[21,22,36-39] These preclinical results suggested that the 3D nanofiber matrices be advanced into the clinical realm, such as for field treatment of junctional hemorrhage and chronic

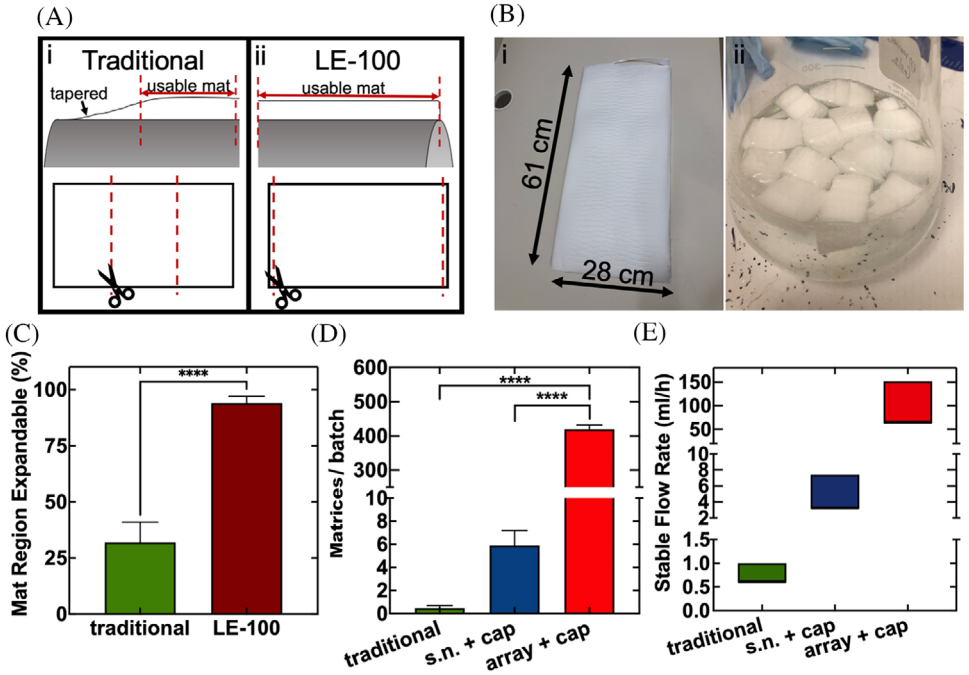

FIGURE 5 Efficiency of production of 3D nanofiber matrices. A, A schematic representing differences in expandable mat area between (i) single nozzle (no lateral movement) and (ii) LE-100 (with lateral movement) electrospinning setups. B, (i) PCL nanofiber mat fabricated with the LE-100 array + caps after removal from rotating drum and (ii) expansion of nanofiber squares into 3D nanofiber matrices in the $NaBH_4$ solution. C, Total expandable nanofiber mat area (%) using single nozzle and array + caps LE-100 electrospinning setups. D, Ranges of maximum stable flow rate at each setup. E, Overall productivity of 3D nanofiber matrices using each setup. ($^{****}P < .0001$). s.n. + cap: single nozzle + cap

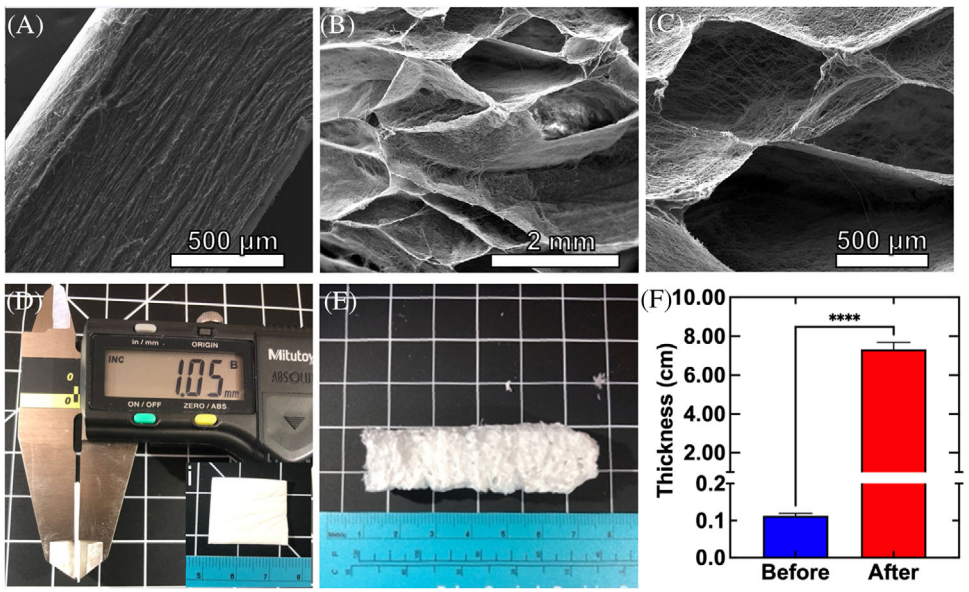

FIGURE 6 Morphology of nanofiber mats produced using the Fluidnatek LE-100 with 3D printed caps on a 20-emitter array before and after expansion and 0.5% gelatin-coating. A, SEM image of LE-100-fabricated nanofiber mat. B, SEM image of the cross section of 3D nanofiber matrices expanded from a LE-100-fabricated nanofiber mat followed by 0.5% gelatin coating. C, High magnification of (B). D, A side (*i.* and front) view of a LE-100-fabricated nanofiber mat. E, A side view of a 3D nanofiber matrice expanded from a LE-100-fabricated nanofiber mat followed by 0.5% gelatin coating. F, Thicknesses of the nanofiber mats before and after expansion. (****$P < .0001$)

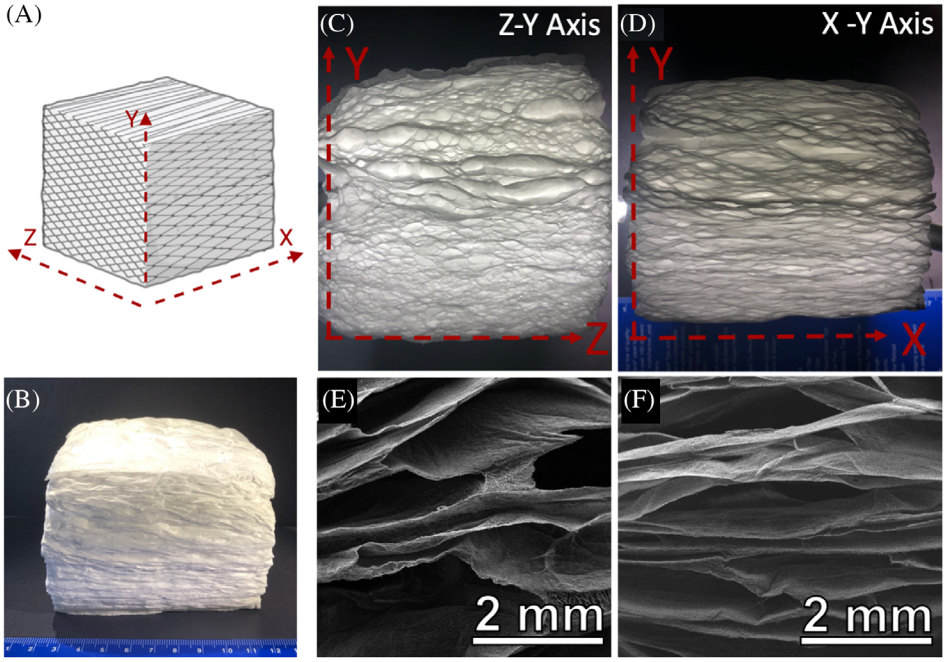

FIGURE 7 Fabrication and characterization of large 3D nanofiber matrices. A, A schematic diagram of the 3D nanofiber matrices with labeled X, Y, and Z coordinates. B, Front camera image (X-Y axis) of 3D nanofiber matrices (roughly 10 cm × 10 cm × 10 cm). C, View of pores along the Z-Y axis and along the (D) X-Y axis. E, SEM images of pores along the Z-Y axis and along the (F) X-Y axis

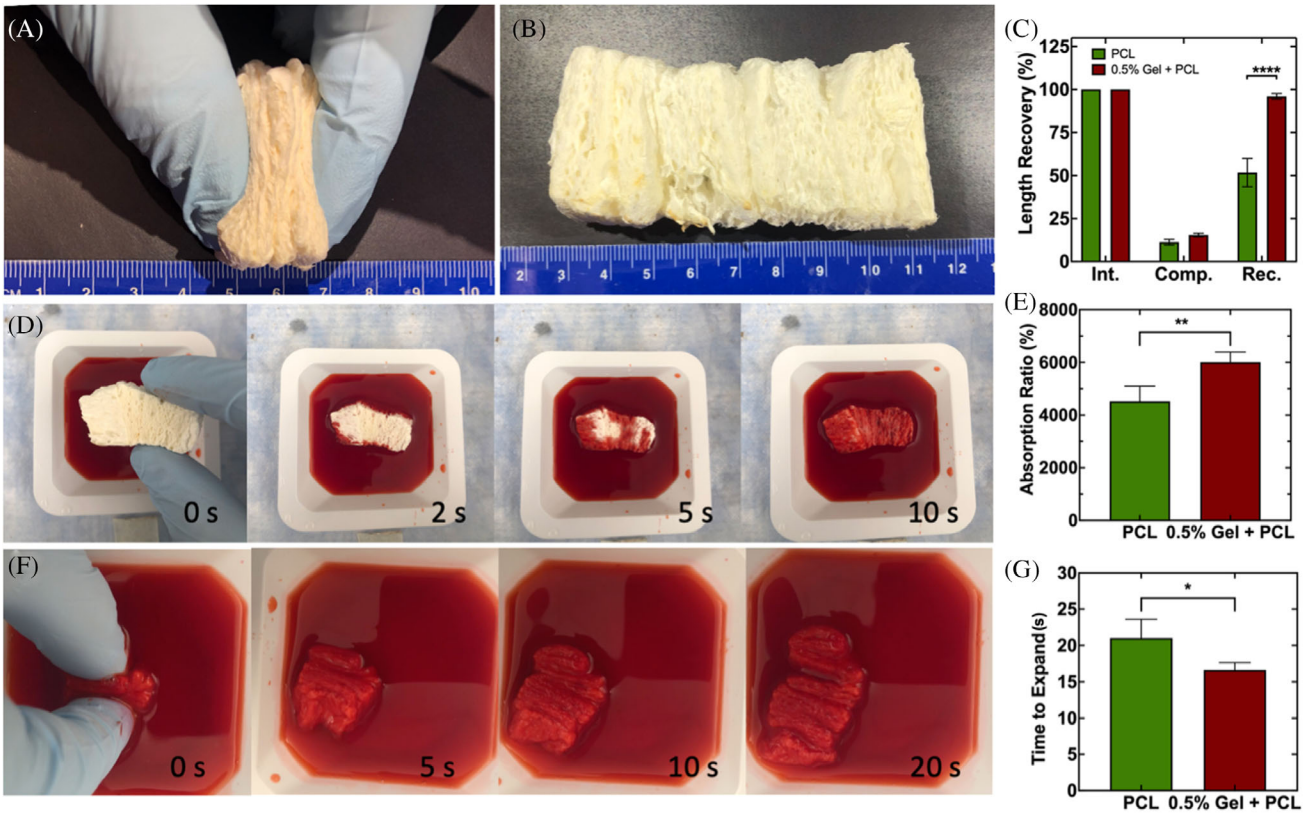

FIGURE 8 Superelastic and absorptive properties of 3D nanofiber matrices produced from scaled-up electrospinning setup. (A & B) Shape recovery of gelatin-coated 3D nanofiber matrices following manual compression. C, Percent length recovery of uncoated and gelatin-coated 3D nanofiber matrices following compression. D, The absorption of BSF for gelatin-coated 3D nanofiber matrices and (E) the absorption ratios of uncoated and gelatin-coated 3D nanofiber matrices. F, Gelatin-coated nanofiber matrices re-expanding in BSF and (G) the time for uncoated and gelatin-coated 3D nanofiber matrices to re-expand in BSF. (*$P < .05$, **$P < .001$, ****$P < .0001$). Int.: initial. Comp.: after compression. Rec.: after recovery. PCL: 3D PCL nanofiber matrices. 0.5%Gel + PCL: 0.5% gelatin-coated 3D PCL nanofiber matrices

wounds. However, the rate of production of 3D nanofiber matrices was too slow to be viable outside of a laboratory setting. Factors hindering the rapid production of nanofiber matrices are the low yield of the single nozzle electrospinning, limited amount of usable nanofiber mat area on the collector, and uncontrolled environmental factors such as humidity and temperature.[40] To increase the production rate of 3D nanofiber matrices, we reported the implementation of modified needle caps and the use of a large-scale electrospinning device consisting of a 20-emitter circular array with a controlled environment.

While the LE-100 offers many controllable parameters, it also introduces a variety of new variables. With precise optimization, the ideal fabrication parameters were established. The addition of the 3D printed needle caps allowed for a stable Taylor cone to form at high flow rates (e.g., 150 mL h^{-1}), resulting in a dramatic increase in the fiber production rate. Fibers produced from the scaled-up setup yielded the similar alignment and morphologies to fibers produced from a single-nozzle electrospinning setup. While an increased flow rate contributed to the increased rate of production, pre-programmed emitter head lateral sweep also allowed for a significantly higher area of usable nanofiber mats to be produced. Because the single-nozzle electrospinning setup often has a stationary needle, the edges of the mat are thinner than the middle, and do not expand to the same length. During cutting, the edges of the mat from the traditional setup are cut off, essentially rendering more than 50% of the mat area worthless. In the LE-100, a lateral sweep moved the emitter head in a left-to-right motion at a uniform rate, thereby ensuring that the entirety of the drum collector as a uniform mat thickness. This allowed for nearly 100% of the mat to be expanded, dramatically increasing the production rate of 3D nanofiber matrices.

Perhaps one of the most important factors in scaling up the production of 3D nanofiber matrices is the applied voltage. Nanofiber mats were fabricated at the flow rate of 150 mL $h^{-1}$when the applied voltages were both 30 and 60 kV (the maximum voltage on an LE-100). Mats produced at 30 kV were not able to sustain expansion when removed from vacuum, returning to squares under atmospheric pressure. SEM examination revealed that a significantly higher number of fibers were not in correct alignment, and also revealed fibers with slightly larger diameters. Under lower voltages, the jet plumes were much wider, which under a single emitter system may not cause problems. Furthermore, the plumes from emitters were crossing, forming fusion points between fibers that acted as meshes that mechanically prevented the expansion of mats into 3D matrices. Once fibers crossed, they fell quickly towards the collector, preventing total solvent evaporation. Under high voltages, plumes seldom contacted, and therefore had minimal fusion, which led to optimal expansion during gas foaming.

Nearly identical morphologies of 3D nanofiber matrices were achieved by the scaled-up setup as by the single nozzle electrospinning setup. Importantly, the gelatin-coated 3D nanofiber matrices produced by the LE-100 exhibited superelasticity, absorptivity, and re-expandability, similar to those produced by the single nozzle electrospinning setup. Additionally, the rate of expansion in BSF confirmed the critical role of gelatin coatings in establishing superelasticity, as gelatin-coated 3D nanofiber matrices were able to re-expand after compression in the BSF solution to a greater degree than uncoated ones, and at a faster expansion rate. The mass production of 3D nanofiber matrices is a critical step for translating their applications and developing an injectable product for treatment of junctional hemorrhage and noncompressible hemorrhage.[22] In addition, 3D nanofiber matrices in a larger size produced by LE100 with modified caps allow for their applications in compressible hemorrhage during elective surgeries as extensive traumatic injuries and elective surgeries often include large areas of bleeding.[21]

4 | CONCLUSIONS

In summary, we have established a suitable system to scale up the production of 3D nanofiber matrices. By using the LE100 electrospinning machine consisting of an array of emitters modified with 3D printed caps, we were able to produce the 3D nanofiber matrices (1 cm × 1 cm × 7 cm) by 875 times faster. Through image analysis, we confirmed that the produced fiber mats had the similar morphology and structure as the ones prepared by the single-nozzle electrospinning setup. Importantly, we demonstrated that the 3D nanofiber matrices produced from the scaled-up method retained the comparable absorptive, re-expansile, and superelastic properties to the ones generated by the single-nozzle electrospinning setup. Having an established means to mass-produce 3D nanofiber matrices will allow for a practical transition from laboratory discovery to preclinical large animal testing, clinical trials, and beyond.

5 | EXPERIMENTAL SECTION

5.1 | Materials

PCL (MW = 80 kDa), gelatin, Pluronic F-127 (F-127), and $NaBH_4$ tablets were all purchased from Sigma-Aldrich (St. Louis, MO). The solvents used, dichloromethane (DCM)

and N, *N*-dimethylformamide (DMF), were purchased from Sigma-Aldrich (St. Louis, MO) and BDH Chemicals (Dawsonville, GA), respectively. Needles (22 gauge) were purchased from McMaster-Carr (Princeton, NJ), a 100 mL glass syringe was purchased from Grainger (Lake Forest, IL), and a Fluidnatek LE-100 electrospininng machine and all attachments were purchased from Bionicia (Valencia, Spain).

5.2 | Traditional fabrication of PCL nanofiber mats

Using a single-nozzle electrospinning setup, electrospun PCL nanofiber mats were fabricated as previously reported.[22] Briefly, 2 g of PCL pellets and 0.2 g of F-127 were completely dissolved in a solution of 16 mL of DCM and 4 mL of DMF (4:1 [v/v]) under gentle spinning. All samples were electrospun using the same stock solution. Approximately 50 mL of the polymer solution was electrospun at room temperature and relative humidity (31%) *via* a single 10 cc syringe with a 22-gauge needle at 0.7 mL h^{-1}, 18 kV, and roughly 18 cm from a grounded drum collector with a 2.5 cm radius and 10 cm length rotating at 1100 rpm. After a roughly 1-mm thick mat was collected, a razor was used to remove the mat from the drum.

5.3 | Fabrication of 3D printed electrospinning caps

Electrospinning caps were printed based on a design inspired by a previous work using a digital light processing (DLP) 3D printer (Vida, EnvisionTEC).[32] The design dimensions were scaled for use on 22-gauge needles. Caps were made of a photocrosslinkable methacrylic-/acrylic resin (Clear Guide, EnvisionTEC) that was crosslinked layer-by-layer to create the full 3D structure. Each cap was designed as a hemisphere with a 3.85 mm diameter and a 0.72 mm channel through the middle. By using 3D printing, many electrospinning caps can be produced at the same time, can be easily cleaned and reused, and were manually added to each 22-gauge needle such that the needle tip was flush with the cap.

5.4 | Determining taylor cone stability

To determine Taylor cone stability at different parameters and under different spinning conditions, a 10% PCL + 1% F-127 polymer solution was spun from a capped or uncapped 20 emitter array in the LE-100 under 30 kV, 65% RH, 25°C, and no lateral sweep. Flow rate was increased from 0 to 200 mL h^{-1}in 4 mL h^{-1} increments. At each increased flow rate, the size, shape, and consistency of the Taylor cone was recorded and qualitatively assigned a value from 0 to 4, with 0 being the least stable to 4 being the most stable. A qualitative ranking of 0 was no spinning, 1 was multiple branching or clogging with minimal spinning, 2 was spinning with multiple branches or frequent dripping/breaking, 3 was consistent spinning with off-centered alignment, and 4 was pristine with ideal cone shape and fiber alignment. An ideal cone shape was considered conical, and a poor cone shape was considered ovular (pendant shaped). At the end of each run, photographs from each flow rate were compared and assessed based on the aforementioned criteria.

5.5 | Scaled-up fabrication of PCL nanofiber mats

Before electrospinning, the 3D printed caps were attached to each needle in the 20-emitter array, with needle tips slightly protruding past the cusp of the cap. The emitters and tubes were flushed with 20 mL of DCM prior to loading the polymer solution. Once the emitter head was loaded with the polymer solution, the 20-emitter circular array with capped 22-gauge needles was used to pump 80 mL of 10% w v^{-1} PCL + 1% w v^{-1} F-127 solution at a flow rate of 150 mL h^{-1}. The potential difference between the spinning head and the drum was 60 kV (+30 kV applied to spinning head, -30 kV applied to drum). The array was 22 cm from the rotating collector (200 rpm, 10 cm diameter, 30 cm length) and moved 160 mm back-and-forth at a rate of 55 mm s^{-1} (x-sweep). The relative humidity was kept at 65%, temperature at 29 °C, and air flow rate at 150 m^3 h^{-1} to ensure all the evaporated DCM was rapidly removed from the spinning chamber. When the polymer solution had only 10 mL remaining, fresh solution was immediately added to the syringe and electrospinning was resumed without stopping drum rotation. Once a 1-mm thick mat was synthesized, it was removed *via* razor blade.

5.6 | Fabrication of 3D nanofiber matrices

The fabrication of 3D PCL nanofiber matrices followed our previous studies.[16,18,19] Briefly, PCL nanofiber mats were submerged in liquid nitrogen and cut into 1 cm by 1 cm squares and submerged in a solution of $NaBH_4$ for 24 hours. After expansion, the nanofiber matrices were washed three times in distilled water and further expanded under vacuum lyophilization until frozen and dry. To ensure the elasticity and shape-recovery of

the PCL nanofiber matrices, a gelatin coating followed by crosslinking was carried out. The expanded 3D PCL nanofiber matrices were immersed in 0.5% w v^{-1} gelatin and freeze-dried until frozen and dry. Optimization of gelatin coatings was previously elucidated and followed in this study.[22] Finally, the gelatin-coated nanofiber matrices were crosslinked in a 25% glutaraldehyde vapor chamber for 12 hours. After removal, the crosslinked nanofiber matrices were stored for further studies. To further demonstrate the ability of the scaled-up mats to expand, radially-aligned PCL objects were fabricated following our previously reported axis-of-rotation technique.[20] Briefly, one side of a pre-cut PCL square was melted on a hot plate and expansion was carried out in the outlined method, expanding the mat into a cylinder (Figure S1).

Nanofiber matrices with a larger dimension were produced using the same methods. The 10 cm × 10 cm squares were cut in liquid nitrogen and expanded in a large bath of a $NaBH_4$ aqueous solution. A flat lid with weight was used to keep the sponge submerged during expansion in the $NaBH_4$ solution. During lyophilization, the sponge was confined to a roughly 12 cm × 12 cm × 12 cm cube mold and expanded *via* vacuum. The sponge was then submerged in a 0.5% w v^{-1} gelatin solution, freeze-dried, and crosslinked following the exact protocol as described for production of small nanofiber matrices.

5.7 | Characterization of morphology and structure

Morphologies of electrospun PCL mats and nanofiber matrices produced from single-nozzle, single nozzle + cap, and scaled-up LE-100 spinning setups (20 emitter array + caps) were imaged by digital cameras and by SEM (FEI, Quanta 200, Oregon, USA). Fiber quality was assessed by morphology and alignment. To measure distribution of both orientation and diameter of electrospun nanofibers, two open-source, validated plugins for Image J were used.[41,42] OrientationJ was used to determine the frequency of fiber angle distribution based on structure tensors, while DiameterJ was used to measure both frequency distribution and variance in nanofiber diameter. Both OrientationJ a DiameterJ are open-source plugins for ImageJ Fiji, an open-source imaging software provided by the National Institute of Health.[43]

Nanofiber matrices (10 cm × 10 cm × 10 cm) were imaged by SEM (FEI, Quanta 200, OR) and digital camera. For camera images, an LED surgical illuminator (LED Fiber Optic Illuminator, Cole-Parmer, Vernon Hills, IL) was used at a minimum setting to illuminate the matrices for pore observation.

5.8 | Determination of scale-up efficiency

The efficiency of the scale-up was analyzed by the number of nanofiber matrices (1 cm × 1 cm × 7 cm) produced per batch at each given setup. First, the ranges of maximum flow rates were recorded on each spinning setup and mats were produced at each setting using single-nozzle, single nozzle + cap, and array + cap settings. Squares of PCL (1 cm × 1 cm) were cut from each mat and expanded as previously reported.[22] The total area of expandable mats was calculated under both conditions and compared. The total number of matrices from a single run were counted and reported on each setup.

5.9 | Expansion and shape recovery analysis

The expansion of 3D nanofiber matrices was measured by comparing the thickness of each PCL square before and after expansion and expressed as a percent of the original thickness. The shape recovery of each matrix was measured by taking width measurements before, during, and after a complete manual compression and allowing re-expansion to occur. The shape recovery after compression was expressed as percent of original length.

5.10 | Compression test

Compression testing on nanofiber matrices produced using a traditional electrospinning set up (single nozzle) and a scaled-up configuration (Fluidnatek LE-100 with multi-emitter array + 3D printed caps). Samples were placed on a universal mechanical testing system (5900 Series Universal Testing Systems up to 50 kN, Instron, Norwood, MA, USA) with two force plates attached. Samples were compressed to 75% for five cycles at 75% compression/min (for example, if the sample was 100 mm long, the compressive rate would be 75 mm/mm/min). Nanofiber matrices were cut to approximately squares prior to compression. Three matrices produced using each configuration were compressed. Maximum load in Newtons was measured and compared.

5.11 | BSF absorption and re-expansion analysis

BSF absorption analysis was carried out by comparing the absorption ratios between coated and uncoated PCL nanofiber matrices produced from a scaled-up setup.

BSF was synthesized as previously reported.[44] The BSF solution contained 0.368 g $CaCl_2$, 8.29 g NaCl in 1000 mL of water and 10 drops of red food coloring (pH 8.2). Briefly, the initial masses of nanofiber matrices from each condition were recorded before being fully submerged in a BSF solution. After 60 seconds, nanofiber matrices were removed and the masses were recorded. The absorption ratio was determined by (Equation 1).

$$Absorption\,Ratio\ (\%) = \frac{W_w - W_d}{W_d} \times 100\% \qquad (1)$$

To determine the rate of expansion in solution, the nanofiber matrices were manually compressed and released while submerged in the BSF. A stopwatch and video recording were used to determine the time for each matrix to re-expand. After full re-expansion in BSF, the final length was taken and reported as a percent of the original length.

5.12 | Statistics

All data is presented as the mean ± standard deviation. All statistical analysis was performed using Graphpad Prism 8.0. Paired t-tests, one-way ANOVA, and frequency distribution (with 2nd order polynomial smoothing) were performed and statistical model assumptions checked following appropriate post hoc testing. Frequency distributions were generated using automatically assigned bins, per DiameterJ and OrientationJ. Statistical significance was considered to be not significant (ns) when $P > .05$, $^{*}P < .05$, $^{**}P < .01$, $^{***}P < .001$, and $^{****}P < .0001$.

ACKNOWLEDGMENTS

This work was partially supported by startup funds from the University of Nebraska Medical Center (UNMC), National Institute of General Medical Science (NIGMS) of the National Institutes of Health under Award Number R01GM123081, Congressionally Directed Medical Research Program (CDMRP)/Peer Reviewed Medical Research Program (PRMRP) FY19 W81XWH2010207, Nebraska Research Initiative grant, and partially supported with resources and the use of facilities at the Omaha VA Medical Center (Nebraska-Western Iowa Health Care System).

DATA AVAILABILITY STATEMENT

Research data are not shared.

ORCID

Jingwei Xie https://orcid.org/0000-0002-8126-1397

REFERENCES

1. J. Xue, T. Wu, Y. Dai, Y. Xia, *Chem. Rev.* **2019**, *119*, 5298.
2. T. S. M. Kumar, K. S. Kumar, N. Rajini, S. Siengchin, N. Ayrilmis, A. V. Rajulu, *Compos. B. Eng.* **2019**, *175*, 107074.
3. C. Zhang, Y. Li, P. Wang, H. Zhang, *Compr. Rev. Food Sci. Food Saf.* **2020**, *19*, 479.
4. W. Zhang, Z. He, Y. Han, Q. Jiang, C. Zhan, K. Zhang, Z. Li, R. Zhang, *Compos. A. Appl. Sci. Manuf.* **2020**, *137*, 106009.
5. S. Chen, J. V. John, A. McCarthy, J. Xie, *J. Mater. Chem. B* **2020**, *8*, 3733.
6. S. Soltani, N. Khanian, T. S. Y. Choong, U. Rashid, *N. J. Chem.* **2020**, *44*, 9581.
7. Kenry, C. T. Lim, *Prog. Polym. Sci.* **2017**, *70*, 1.
8. R. Nayak, R. Padhye, I. L. Kyratzis, Y. B. Truong, L. Arnold, *Text. Res. J.* **2011**, *82*, 129.
9. B. A. Blakeney, A. Tambralli, J. M. Anderson, A. Andukuri, D. J. Lim, D. R. Dean, H. W. Jun, *Biomaterials* **2011**, *32*, 1583.
10. G. Jin, M Shin, S. H. Kim, H. Lee, J. H. Jang, *Angew. Chem. Int. Ed.* **2015**, *54*, 7587.
11. S. Jeong, N. A. Burns, C. A. Bonino, I. K. Kwon, S. A. Khan, E. K. Alsberg, *J. Mater. Chem. B* **2014**, *2*, 8116.
12. J. B. Lee, S. I. Jeong, M. S. Bae, D. H. Yang, D. N. Heo, C. H. Kim, *Tissue Eng. A* **2011**, *17*, 2695.
13. B. M. Baker, R. P. Shah, A. M. Silverstein, J. L. Esterhai, J. A. Burdick, R. L. Mauck, *Proc. Natl. Acad. Sci. U S A* **2012**, *109*, 14176.
14. S. Cai, H. Xu, Q. Jiang, Y. Yang, *Langmuir* **2013**, *29*, 2311.
15. C. A. Bonino, K. Efimenko, S. I. Jeong, M. D. Krebs, E. Alsberg, S. A. Khan, *Small* **2012**, *8*, 1928.
16. J. Jiang, M. A. Carlson, M. J. Teusink, H. Wang, M. R. MacEwan, J. Xie, *ACS Biomater. Sci. Eng.* **2015**, *1*, 991.
17. M. K. Joshi, H. R. Pant, A. P. Tiwari, H. J. Kim, C. H. Park, C. S. Kim, *Chem. Eng. J.* **2015**, *275*, 79.
18. J. Jiang, Z. Li, H. Wang, Y. Wang, M. A. Carlson, M. J. Teusink, M. R. MacEwan, L. Gu, J. Xie, *Adv. Healthcare Mater.* **2016**, *5*, 2993.
19. J. Jiang, S. Chen, H. Wang, M. A. Carlson, A. F. Gombart, *Acta Biomater.* **2018**, *68*, 237.
20. S. Chen, H. Wang, A. McCarthy, Z. Yan, H. J. Kim, M. A. Carlson, Y. Xia, J. Xie, *Nano Lett.* **2019**, *19*, 2059.
21. S. Chen, J. V. John, A. McCarthy, M. A. Carlson, X. Li, J. Xie, *Appl. Phys. Rev.* **2020**, *7*, 021406.
22. S. Chen, M. A. Carlson, Y. S. Zhang, Y. Hu, J. Xie, *Biomaterials* **2018**, *179*, 46.
23. S. Chen, A. McCarthy, J. V. John, Y. Su, J. Xie, *Adv. Mater.* **2020**, *32*, 2003754.
24. J. Xie, X. Li, Y. Xia, *Macromol. Rapid Commun.* **2008**, *29*, 1775.
25. J. S. Varabhas, G. G. Chase, D. H. Reneker, *Polymer* **2008**, *49*, 4226.
26. P. Vass, E. Szabo, A. Domokos, E. Hirsch, D. Galata, B. Farkas, B. Demuth, S. K. Andersen, T. Vigh, G. Verreck, G. Marosi, Z. K. Nagy, *WIREs Nanomed. Nanobiotechnol.* **2020**, *12*, e1611.
27. L. Persano, A. Camposeo, C. Tekmen, D. Pisignano, *Macromol. Mater. Eng.* **2013**, *298*, 504.
28. P. Pokorny, E. Kostakova, F. Sanetrnik, P. Mikes, J. Chvojka, T. Kalous, M. Bilek, K. Pejchar, J. Valtera, D. Lukas, *Phys. Chem. Chem. Phys.* **2014**, *16*, 26816.
29. J. Valtera, T. Kalous, P. Pokorny, O. Batka, M. Bilek, J. Chvojka, P. Mikes, E. K. Kostakova, P. Zabka, J. Ornstova, J. Beran, A. Stanishevsky, D. Lukas, *Sci. Rep.* **2019**, *9*, 1801.

30. J. Xue, T. Wu, Y. Xia, *APL Mater*. **2018**, *6*, 120902.
31. J. Xie, M. R. MacEwan, A. G. Schwartz, Y. Xia, *Nanoscale* **2010**, *2*, 35.
32. M. R. Morad, A. Rajabi, M. Razavi, S. R. P. Sereshkeh, *Sci. Rep.* **2016**, *6*, 38509.
33. F. Cruz-Mazo, M. O. Wiedorn, M. A. Herrada, S. Bajt, H. N. Chapman, A. M. Gañán-Calvo, *Phys. Rev. E.* **2019**, *100*, 031101
34. J. Kim, S. Bui Quang Tran, B. Seong, H. Lee, G. Kang, J. Hwan, D. Byun, *J. Vis.* **2020**, *23*, 449–457.
35. A. L. Yarin, S. Koombhongse, D. H. Reneker, *J. Appl. Phys.* **2001**, *90*, 4836.
36. J.J. Harris, S. Lu, P. Gabriele, *Polym. Int.* **2018**, *67*, 969.
37. K. Zhang, X. Bai, X. Cao, X. Jiao, Y. Li, Y. Qin, Y. Wen, X. Zhang, *Biomaterials* **2019**, *204*, 70.
38. F. Rao, Z. Yuan, M. Li, F. Yu, X. Fang, B. Jiang, Y. Wen, P. Zhang, *Artif. Cells Nanomed. Biotechnol.* **2019**, *47*, 491.
39. S. Chen, H. Wang, Y. Su, J. V. John, A. McCarthy, S. L. Wong, J. Xie, *Acta Biomater*. **2020**, *108*, 153.
40. E. Yang, J. Shi, Y. Xue, *J. Appl. Polym. Sci.* **2010**, *116*, 3688.
41. N. A. Hotaling, K. Bharti, H. Kriel, C. G. Simon, *Biomaterials* **2005**, *61*, 327.
42. R. Rezakhaniha, A. Agianniotis, J. T. C. Schrauwen, A. Griffa, D. Sage, C. V. C. Bouten, F. N. van de Vosse, M. Unser, N. Stergiopulos, *Biomecch. Model Mechanobiol.* **2012**, *11*, 361.
43. J. Schindelin, I. Arganda-Carreras, E. Frise, V. Kaynig, M. Longair, T. Pietzsch, C. Rueden, S. Saalfeld, B. Schmid, J. Y. Tinevez, D. J. White, V. Hartenstein, K. Eliceiri, P. Tomancak, A. Cardona, *Nat. Methods.* **2012**, *9*, 676.
44. H. Derakhshandeh, F. Aghabaglou, A. McCarthy, A. Mostafavi, C. Wiseman, Z. Bonick, I. Ghanavati, S. Harris, C. Kreikemeier-Bower, S. M. Moosavi Basri, J. Rosenbohm, R. Yang, P. Mostafalu, D. Orgill, A. Tamayol, *Adv. Funct. Mater.* **2020**, *30*, 1905544.

SUPPORTING INFORMATION

Additional supporting information may be found online in the Supporting Information section at the end of the article.

How to cite this article: McCarthy A, Saldana L, McGoldrick D, et al. Large-scale synthesis of compressible and re-expandable three-dimensional nanofiber matrices. *Nano Select*. **2021**;*2*:1566–1579. https://doi.org/10.1002/nano.202000284